Weber, T., Thomas, M. (2017): Tidal dynamics and their influence on the climate system from the Cretaceous to present day. - *Global and Planetary Change*, *158*, pp. 173—183.

DOI: http://doi.org/10.1016/j.gloplacha.2017.09.019

Tidal dynamics and their influence on the climate system from the Cretaceous to present day

T. Weber[1,*], M. Thomas[1,2]

[1]GFZ German Research Centre for Geosciences, 14473 Potsdam, Germany
[2]Institute of Meteorology, Freie Universität Berlin, 12165 Berlin, Germany
*Corresponding author

This manuscript was originally published in Global and Planetary Change. Please cite as: Weber, T., Thomas, M. (2017): Tidal dynamics and their influence on the climate system from the Cretaceous to present day. - *Global and Planetary Change*, 158, pp. 173—183. DOI: http://doi.org/10.1016/j.gloplacha.2017.09.019

Tidal dynamics and their influence on the climate system from the Cretaceous to present day

T. Weber[1,*], M. Thomas[1,2]

[1]GFZ German Research Centre for Geosciences, 14473 Potsdam, Germany
[2]Institute of Meteorology, Freie Universität Berlin, 12165 Berlin, Germany
*Corresponding author

Global numerical ocean models used for paleo-climate reconstructions commonly only consider the ocean's general circulation but neglect tidal dynamics. However, tidal dynamics affect the ocean's mean general circulation, in particular by vertical mixing and tidal residual mean currents. Through feedback loops the whole climate system is affected.
Plate tectonics modify geometric resonance conditions in ocean basins and thereby tidal dynamics. We study the influence of ocean tides on the ocean general circulation and atmospheric parameters by forcing the coupled atmosphere-ocean model ECHAM5/MPIOM with the complete lunisolar tidal potential. Simulations have been performed for five tectonically important time-slices: the Early Albian (ca. 110 million years ago, Ma), the Cenomanian-Turonian Boundary (ca. 93 Ma, CTB), the Early Eocene (ca. 55 Ma), the Early Pliocene (ca. 3.5 Ma), and a pre-industrial period (ca. 1850 AD). The model results suggest that the global mean tidal potential energy in the Early Eocene is almost three times larger than in the CTB. The large potential energy input in the Early Eocene leads to a tripling of current velocities in 10% of the deep ocean. Although the effect of tides on the general ocean circulation is less pronounced in the other time-slices, horizontal velocities are modified by more than 20% in 55% of the deep ocean.
The tidally induced shifts of ocean currents and vertical mixing also have an effect on the three-dimensional temperature distribution in the ocean. The impact of tidal dynamics on atmospheric temperatures is particularly strong in the Southern Ocean of the Early Pliocene and the pre-industrial period. By a feedback loop with the atmosphere, tidal forcing locally reduces sea-ice concentration by up to 30% and local atmospheric 2 m temperatures by up to 4°C.
Although uncertainties in bathymetry reconstructions limit the significance of quantitative analysis, the qualitative conclusions suggest that the impacts of ocean tides on climate reach an order of magnitude, which require its consideration as additional uncertainty in the interpretation of paleo-climate studies. However, the impact of ocean tides has specific characteristics in each time-slice hampering its simple parametrization.

Keywords: tides, paleoclimatology, ocean modelling

1 Introduction

Ocean circulation models used for paleo-climate simulations generally do not include tidal effects. It is implicitly assumed that the two main components of ocean dynamics, i.e., the ocean's general circulation and tidal dynamics, are completely independent. However, tidal forcing can change the ocean's general circulation in different ways. (1) Transport ellipses induced by tidal constituents are distorted by non-linear effects, such as bottom friction, and tidal residual mean currents (TRMC) are induced. These are of major importance in shallow water and close to the ocean bottom (e.g., Schiller (2004)). (2) The barotropic tide is partially converted to baroclinic or internal tide through friction and flow over rough topography. Thereby vertical mixing is enhanced, which is reflected in ocean models as an increase in vertical diffusivity (e.g., Wunsch (2002); Müller et al. (2010)). (3) Vertical mixing is also increased by a larger vertical velocity shear.

TRMC directly interact with the general circulation and can shift thermohaline or wind driven currents and change their velocities. This alters shear stress on sea ice and advection of heat and salt. Increased vertical mixing affects the three-dimensional temperature distribution in the ocean (e.g., Lee et al. (2006); Brierley and Fedorov (2011)). Thereby also the density distribution and hence deep water formation and the thermohaline circulation are altered (e.g., Schiller (2004)). Furthermore, conditions for the formation of sea ice are modified, affecting both sea ice concentration and thickness (Koentopp et al. (2005)). Changed surface conditions interact with the atmosphere and impact atmospheric temperatures, pressure systems, winds, precipitation, albedo, etc. (Müller et al. (2010); Brierley and Fedorov (2011)). The atmosphere couples back to the ocean by means of energy, momentum and mass fluxes and induces further alterations in ocean dynamics. The nonlinear feedback loops between atmosphere and ocean and within each system transform the periodic, high frequency influence of oceanic tides to long-lasting modifications of the climate system (Wunsch (2002); Müller et al. (2010); Brierley and Fedorov (2011)).
However, the nonlinearity of these interactions makes it difficult to identify which mechanism is responsible for each alteration in the ocean. This problem is amplified by coupling the ocean general circulation model (OGCM) to an atmosphere general circulation model (AGCM), because additional feedbacks between atmosphere and ocean have to be taken into account. For this reason we mainly describe the effects of including tidal forcing into the ocean model and only occasionally identify specific physical process chains responsible for modifications.
Including tidal effects into ocean standalone models or coupled atmosphere-ocean models can reduce the root mean square errors of the simulated currents and surface temperatures in comparison to *in-situ* measurements (Lee et al. (2006); Müller et al. (2010)). Müller et al. (2010) also observed a more accurate representation of the North Atlantic Current when including tides into the model ECHAM5/MPIOM: the North Atlantic Current is strengthened by tidal dynamics. This way, a stronger northward heat transport is induced which increases sea surface temperatures in the North Atlantic and reduces the root mean square error of sea surface temperatures in comparison to observational data.

On geological timescales, ocean dynamics are controlled by tectonic processes. Firstly, the opening and closing of seaways significantly affects water mass exchange between ocean basins and, thus, large-scale heat transports. Secondly, resonance conditions of ocean tides are especially sensitive to the geometry of ocean basins which evolves due to tectonic movement of continents, opening and closing of throughflows, the deepening of the ocean and evolution of sea ice coverage. A recent study by Wunsch (2016) studies the effects of tides on snowball Earth and shows that time-mean TRMC could have had a similar magnitude to that of geothermal

heating driven circulation. The effect of evolving geometry of ocean basins on the main lunar tidal constituent M_2 is studied by Gotlib and Kagan (1985) for nine time-slices from the Early Cambrian (542–513 million years ago, Ma) to present day. They found large amplitudes from the Early Cambrian to the Late and Middle Ordivician (472–444 Ma), and from the Middle and Late Jurassic (176–146 Ma) to present day. In between, from the Early and Middle Devonian (416–385 Ma) to the Triassic (250–200 Ma), amplitudes of the M_2 tide are significantly smaller, accompanied by a strong decrease of potential tidal energy. According to a case study by Brierley and Fedorov (2011) for the Pliocene, tidally altered vertical mixing modifies ocean circulation, sea surface temperatures and climate. Tidally increased diffusivity could also increase the meridional overturning circulation and thereby the meridional heat transport. Thomas et al. (2014) found this to be a possible contribution to the reduction of the equator-to-pole temperature gradient in the Early Eocene when increasing vertical diffusivity in the MITgcm. However, Weber and Thomas (2017) found no significant increase in meridional heat transport due to tidal forcing in their simulation of Early Eocene ocean dynamics. For the last glacial maximum (LGM) two different results are obtained. While Montenegro et al. (2007) did not find a clear correlation between increased diffusivity and the strength of the meridional overturning circulation, Schmittner et al. (2015) find an acceleration of the meridional overturning circulation of 21-46% due to increased vertical diffusivity. Also Wunsch (2005) concluded that during the Younger Dryas ($\approx$ 12,000 years before present) de-glaciation shifted abyssal mixing and thereby altered oceanic meridional heat transport.

Until now, studies of the effect of tides on paleo-oceans either solely consider tidal dynamics in a simplified ocean (e.g., Gotlib and Kagan (1985); Griffiths and Peltier (2009); Green and Huber (2013)) or the effects of tides are parametrized (e.g., Montenegro et al. (2007); Brierley and Fedorov (2011); Thomas et al. (2014)). Due to the importance of tidal dissipation to the evolution of the Earth-Moon system (Laskar et al. (2004)) the main objective of most studies was the determination of the global mean dissipation rate over time. For these reasons, the interaction of tidal dynamics and the ocean's general circulation is not well understood for paleo-oceans. In order to fill this gap, we examine the influence of ocean tides on velocities, surface temperatures and sea ice. We simultaneously model tidal dynamics and the atmosphere-ocean general circulations for five time-slices ranging from the Early Albian (112–109 Ma) in the Cretaceous to present day with the coupled atmosphere-ocean model ECHAM5/MPIOM. The considered five time-slices represent major tectonic key events affecting ocean circulation. These are the Early Albian (ALB), the Cenomanian-Turonian Boundary (CTB, 93 Ma), the Early Eocene (EE, 54.8–49.0 Ma), the Early Pliocene (PLIO, 5.3–3.6 Ma), and a pre-industrial period (PI, 1850 AD). Africa and South America started their tectonic breakup during the Early Cretaceous, resulting in a narrow South Atlantic that was separated from the North Atlantic by a landbridge between Africa and South America during the Early Albian. Furthermore the Drake Passage was open and allowed the throughflow of intermediate waters; India was separated from Africa and Antarctica while Australia was still connected to Antarctica. In the following 17 million years, Africa and South America drifted further apart, thereby connecting the South Atlantic to the North Atlantic. A southward drift of the South American plate closed the Drake Passage during the Paleocene, separating the Pacific from the South Atlantic during the Early Eocene. Between the Early Eocene and the Late Oligocene (54.8–23.8 Ma) the Drake Passage and Tasman Passage opened, enabling the existence of the Antarctic Circumpolar Current (ACC). Furthermore, the Tethys Sea closed during this time, leaving the North Atlantic separated from the Pacific Ocean until the Early Pliocene. During the Early Pliocene the Central American Seaway closed, connecting North and South America by a landbridge.

The tectonic evolution of oceanic gateways and ocean basin geometry affects resonance conditions in the ocean and thereby tidal dynamics in the ocean. The evolution of the tidal system

over the last 110 Ma will be studied in section 3.1. Since tidal forcing directly affects horizontal velocities and hereby indirectly near-surface temperatures in ocean and atmosphere and sea ice concentration, the tidal influence on these variables is analyzed in sections 3.2 and 3.3. We end with a discussion and conclusions in sections 4 and 5.

2 Models and boundary conditions

The coupled atmosphere-ocean model ECHAM5/MPIOM (Roeckner et al. (2003, 2004); Marsland et al. (2003)) is used to simulate the five aforementioned time-slices. The atmosphere model ECHAM5 uses the horizontal resolution T31 ($\sim$3.75°×3.75°) and 19 vertical hybrid sigma/pressure levels. The ocean model MPIOM has a horizontal resolution of $\sim$3.0°×1.8° and 20 unevenly distributed vertical levels (GR30L20). The tidal module calculates the complete lunisolar tidal potential with an ephemeris approach (Duffett-Smith (1986); Thomas et al. (2001)). No parametrization for the conversion of barotropic tide to internal tide is used. Consequences and limitations originating hereof are discussed in section 4.

The boundary conditions for the Early Albian and the CTB are based on reconstructions of topography, bathymetry and vegetation by Sewall et al. (2007). The boundary conditions for the Early Eocene are from Sewall et al. (2000) and Huber and Sloan (2001). In accordance with proxy data (cf., Haworth et al. (2005); Aucour et al. (2008); Fletcher et al. (2008); Passalia (2009); Hong and Lee (2012); Royer (2014); Pearson and Palmer (2000); Royer et al. (2001); Royer (2006); Zeebe et al. (2009)), an atmospheric CO_2 concentration of 450 ppm is prescribed in these three simulations. The boundary conditions for the Early Pliocene follow the Pliocene Model Intercomparison Project (PlioMIP, Haywood et al. (2010)). An atmospheric CO_2 concentration of 400 ppm is prescribed (Haywood et al. (2010) and references therein). The boundary conditions for the pre-industrial period are based on experiment mil0001 (Jungclaus (2007)) of the Millennium Experiments performed by the Max Planck Institute for Meteorology. The CO_2 concentration is set to 278 ppm. All simulations include a vegetation distribution based on reconstructions.

The model is run for 1500 years without tidal forcing for every time-slice. At this point a quasi-equilibrium is reached (Weber (2016); Weber and Thomas (2017)). For the following years a parametrization of the potential of loading and self-attraction (LSA) according to Accad and Pekeris (1978) is included into the ocean model in the form

$$\Phi_{LSA} = g\zeta \int_{-h}^{\eta} \frac{\rho(z)}{\rho_0} \mathrm{d}z, \tag{1}$$

where g is the mean gravitational acceleration, $\zeta = 0.1$ a proportionality factor (Parke (1982)), η the instantaneous, local sea surface elevation, h the ocean depth, ρ the instantaneous, local density, ρ_0 a reference density, and z the vertical coordinate. For each time-slice (ALB, CTB, EE, PLIO, PI) two simulations with a duration of 100 years each are undertaken after the run-up (model years 1500-1599): one simulation neglects (named ALBCTRL, CTBCTRL, EECTRL, PLIOCTRL, PICTRL) and one considers tidal forcing (named ALBTIDE, CTBTIDE, EETIDE, PLIOTIDE, PITIDE). The analyzes presented here are based on the time average over the last 50 years of each model run (years 1550-1599).

We determine statistical significance of tidally induced modifications by the z-test. The z-value for every variable at every location is calculated in dependence of the standard deviation of the decadal means of the simulation years 1550-1599 of CTRL. The tidal influence on a variable will

be called statistically significant if the variable has a z-value larger than 2.58 and lies therefore in the 99% confidence interval. All results shown in this study are statistically significant and regions of non-significant influences of tidal forcing are represented in the figures in white.

A comparison of the pre-industrial tidal system to the ocean bottom pressure dataset by Ray (2013) gives a root mean square error of 14.5 cm and 7.4 cm for the M_2 and K_1 tides, respectively. Considering the coarse spatial resolution required for paleo-modelling, this is a reasonable representation of the global tides in comparison to other models (e.g., Müller et al. (2010)). The Atlantic meridional overturning circulation is simulated in PICTRL with a vertically integrated transport and standard deviation of 16.7±0.7 Sv at 26°N, while a multi-annual mean transport of 17.2±0.9 Sv is measured by McCarthy et al. (2015). Also the transport by the ACC is with a simulated value of 129±5.4 Sv in accordance with measurements of 134±11.2 Sv (Cunningham et al. (2003)). The model gives thus a realistic representation of the ocean's dynamics. A more extensive evaluation of the model setup for the pre-industrial period and the paleo time-slices can be found in Weber (2016) and Uenzelmann-Neben et al. (2016).

3 Results

3.1 Tidal dynamics over time

Tectonic variation of resonance conditions in ocean basins affect amphidromic systems of all tides constituents. However, largest amplitudes are simulated in all five time-slices for the semi-diurnal lunar tide M_2 which in the global mean is responsible for approximately 25% of the total tidal amplitude in all time slices. Its influence is therefore almost twice as large as for the second largest tidal constituent. This is O_1 for PITIDE, with a share of almost 17% in the total tidal variation of sea surface height, and K_1 for the other time-slices with a contribution between 12% (in CTBTIDE) and 16% (in PLIOTIDE). For this reason, only the tide M_2 will be considered in this section.

The Early Albian is characterized by the vast Pacific Ocean that is connected by the broad Indo-Pacific Throughflow (IPT) to the Indian Ocean (cf., fig. 1). The remaining oceans — South Atlantic, North Atlantic, Tethys Sea and Arctic Ocean — are small and shallow. The oscillation system in the Early Albian Atlantic Ocean is characterized by numerous amphidromic points of the M_2 tide with amplitudes generally smaller than 50 cm (figure 1). In the Pacific Ocean, on the other hand, only few amphidromic points develop and amplitudes of up to 2 m are simulated at the North American, Asian and Australian coasts. The central Pacific is marked by two maximum amplitudes of up to 1 m. In the Indian Ocean only amphidromic points with small oscillating systems develop, while tidal waves from the Pacific Ocean propagate through the Indo-Pacific Gateway into the Indian Ocean. The Tethys Sea is in the Early Albian very shallow, which prevents the formation of large oscillating systems (Archer (1996)). The Tethys Sea and the adjacent proto-Fram and Turgay Straits are thus marked by numerous amphidromic points that are surrounded by Kelvin waves with amplitudes smaller than 30 cm.
Until the CTB, South America and Africa had broken apart, thus connecting North and South Atlantic (Sewall et al. (2007)). Furthermore, various epicontinental seas formed (White et al. (2000)). However, the tidal system in the CTB resembles the tidal system in the Early Albian. In the newly formed epicontinental seas numerous oscillating systems with small amplitudes develop.
The tidal system changes considerably until the Early Eocene. The closure of the Drake Passage (Lawver and Gahagan (2003); Livermore et al. (2005); Ghiglione et al. (2008)) inhibits the propagation of tidal waves from the South Atlantic to the Pacific and results in the formation of Kelvin waves at the Antarctic coasts. Consequently, amplitudes of more than 1 m are simulated

in EETIDE. Large amplitudes also affect the IPT north of Australia with amplitudes of more than 3 m. For the first time, resonance conditions in the South Atlantic favor semi-diurnal tidal constituents and lead to amplitudes larger than 1 m at the South American and African coasts. The opening of the Drake Passage until the Early Pliocene reduces the tidal amplitudes at the Antarctic coast and leaves only a remnant of the former high amplitudes in the Weddell Sea, where values of up to 1.4 m are simulated in PLIOTIDE. The westward shift of North and South America enlarges the North and South Atlantic and shrinks the Pacific Ocean. This leads to resonance conditions favorable for M_2 in the North Atlantic and increases amplitudes at the coasts of Europe and Greenland. In the Pacific Ocean, on the other hand, amplitudes are reduced at the Asian coast and in the central Pacific.
The pre-industrial bathymetry differs from the Early Pliocene mainly in the closed Central American Seaway. This creates a new amphidromic point in the pre-industrial southern North Atlantic and makes the amphidromic point in the tropical East Pacific disappear. Amplitudes at the Brazilian coast are reduced from 1 m to less than 50 cm.

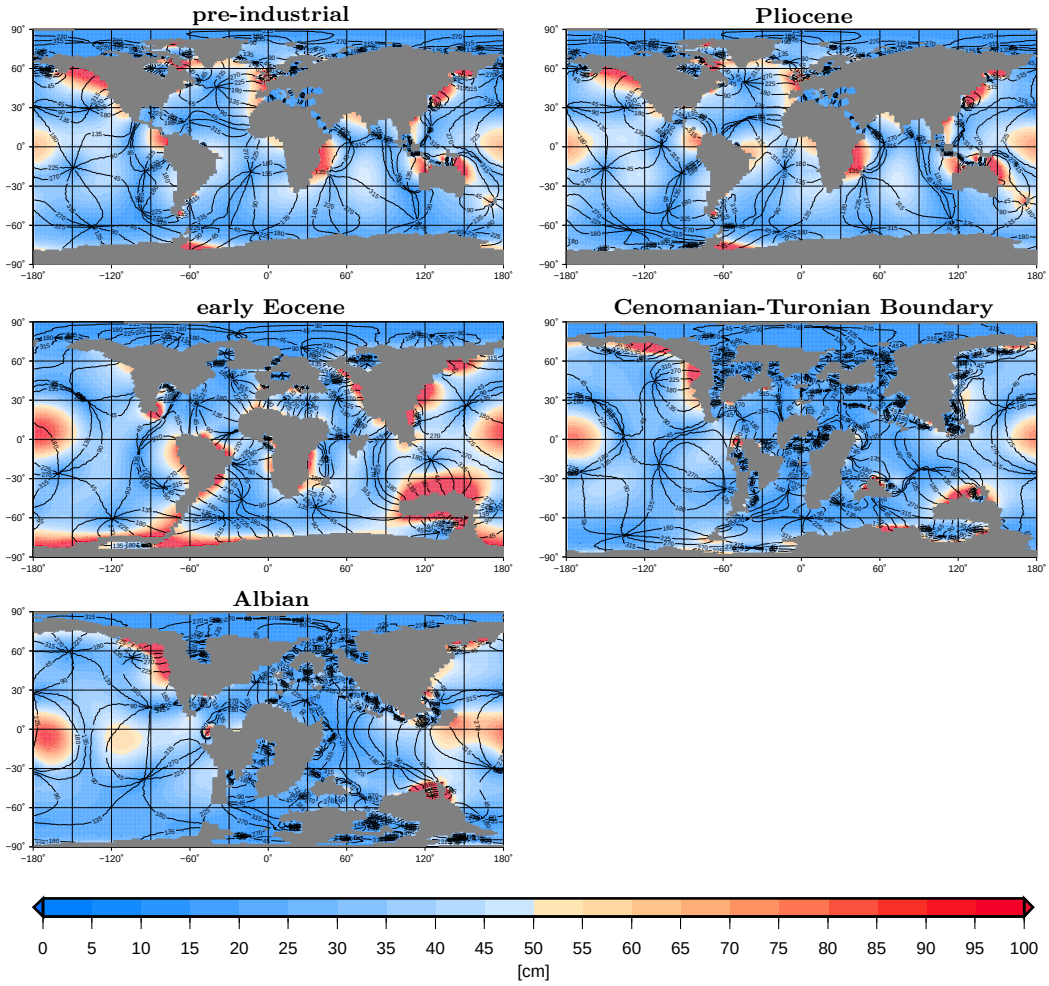

Figure 1: Amplitude (colored contours) and phase (numbered lines in °) of the M_2 tide calculated by least square errors from the simultaneous runs of circulation and ephemeris tides for the pre-industrial, the Early Pliocene, the Early Eocene, the CTB and the Early Albian.

In order to objectively compare the amplitudes of the main tidal constituent of the five time-slices, the tidal potential energy (TPE) is defined as

$$\mathrm{TPE} = g\, m\, A_{X_i} = g\ (\rho_0\, \Delta x\, \Delta y\, A_{X_i})\ A_{X_i} \sim\ A_{X_i}^2 \tag{2}$$

where g is the gravitational acceleration, m is the vertically displaced mass, A_{X_i} the amplitude of a tidal constituent X_i, $\rho_0 = 1035\,\mathrm{kg\,m^{-3}}$ an assumed constant density of the ocean, and Δx and Δy the horizontal extents of a model's grid box in zonal and meridional direction, respectively. The TPE is therefore proportional to the square of the tidal amplitude.

In figure 2 values of the global mean TPE are given for the tides M_2, S_2, O_1, K_1 and the sum over the 17 major tidal constituents for the five time-slices. The magnitudes of both the total TPE and the contribution of individual tidal constituents to the total TPE reflect the dependence of the tidal oscillation systems on prevailing geometric resonance conditions. Largest TPE is induced in the Early Eocene with a total of 2025 PJ, what is almost three times the energy input of the CTB (approximately 719 PJ). It can therefore be expected that the impact of tides on the ocean general circulation is largest in the Early Eocene. While M_2 has the largest contribution to the total TPE in all time-slices, the relative importance of other tidal constituents differ. In the CTB O_1 has with 56 PJ the smallest contribution to the total energy input, while in all other time-slices it is S_2 with values ranging from 77 to 217 PJ. Another interesting feature is that only in the present-day run the O_1 energy contribution is significantly larger than that of K_1 indicating that present-day conditions cannot be simply transferred to paleo-oceans and that small differences in boundary conditions between PITIDE and PLIOTIDE significantly influence the tidal oscillation systems.

3.2 The influence of tides on circulation induced velocities

Several studies have demonstrated that the nonlinear interaction between tidally induced diffusivity, bottom friction and vertical mixing alter the direction and strength of ocean currents (e.g., Moon (2005); Müller et al. (2010)). Thereby the model's representation of velocities, sea surface temperature and sea surface salinity can be improved in comparison to measurements

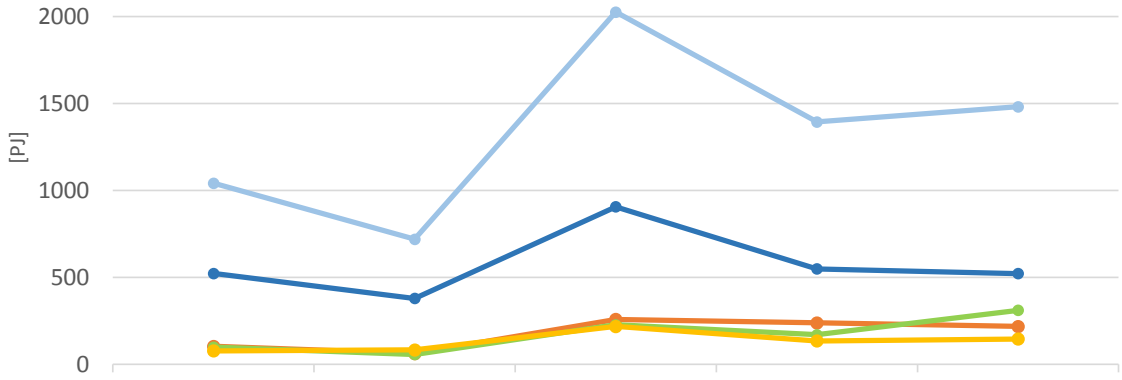

	ALB	CTB	EE	PLIO	PI
M2	522	378	905	548	521
K1	103	62	258	238	217
O1	98	56	227	170	310
S2	77	82	217	134	145
total	1041	719	2025	1393	1481

Figure 2: Tidal potential energy in [PJ] of the Early Albian (ALB), Cenomanian-Turonian Boundary (CTB), Early Eocene (EE), Early Pliocene (PLIO) and pre-industrial period (PI).

(e.g., Lee et al. (2006); Müller et al. (2010)). In this section, we will describe the tidally induced modifications of the ocean's currents as absolute differences TIDE-CTRL and relative variations TIDE/CTRL of the 50-year mean of horizontal velocities.

The absolute differences are larger above 1000 m depth than below 1000 m in all time-slices (cf., figures 3 and 4). In contrast, velocities are altered by more than 20% in less than 30% of the upper ocean in all time-slices except the Early Eocene (cf., figures 3), while in at least 55% of the lower ocean a velocity alteration of more than 20% is simulated for all time-slices. Due to this inherent separation at a depth of approximately 1000 m, the following analysis of the ocean is separated in the upper ocean (from the surface to 1000 m depth) and the lower ocean (below 1000 m depth).

The Early Albian is the time-slice with the lowest rate of significant velocity differences between ALBTIDE and ALBCTRL in the deep ocean (73%). It is also the only time-slice with a significant reduction of velocities in the lower ocean. Velocities are significantly reduced by more than 20% in 16% of the lower ocean. This is mainly the case in the IPT and the southwestern Pacific. An eastward current transports waters from the Indian Ocean through the IPT into the Pacific Ocean at 10°S. This current's velocity is reduced by 0.2 cm/s, or equivalently 50% (cf., figure 4). This might be due to tidal waves propagating from the Pacific Ocean into the Indian Ocean In the southeastern Pacific the general ocean circulation is directed eastward at 40°–50°S. This current bifurcates at 100°W into a northward and a southward component. While the northward component is strengthened by 250–300%, the southward component is weakened by 30–50%. The prevailing ocean circulation in the northeastern Pacific is increased by 100–200%.

The reduction of velocities simulated in the Early Albian IPT is not existent in the CTB. An amphidromic point has formed in the Indian Ocean and counteracts the amphidromic system in the Pacific Ocean. Hence, tidal waves propagate with less velocity from the Pacific into the Indian Ocean. Although absolute differences in velocities rarely exceed 0.1 cm/s, almost 30% of the lower ocean are significantly increased by more than 50% in CTBTIDE. This is due to a shallow thermohaline circulation in the CTB with slow currents in the lower ocean. Similar to ALBTIDE, a relative increase in velocities is simulated in CTBTIDE mainly in the northeastern Pacific.

The Early Eocene is the time-slice with the highest rate of significant velocity changes in the deep ocean (over 90%). In addition, strongest relative modification of horizontal velocities are simulated in the Early Eocene. In more than 35% of the deep ocean, velocities are significantly increased by more than 100%; in 10% of the lower ocean an increase by more than 200% is simulated. The thermohaline circulation in the Early Eocene is very shallow (Lunt et al. (2012); Weber (2016)) and bottom velocities rarely exceed 1.5 cm/s. The velocities of the TRMCs therefore generally exceed the velocities of the general ocean circulation in the lower ocean. An increase of more than 0.5 cm/s is simulated in the IPT and the Central American Seaway. Although a reduction of velocities of up to 0.3 cm/s is simulated in the Weddell Sea, the relative changes are less than 20%.

In the Early Pliocene the absolute variation of velocities is mainly located to the Southern Ocean, where the Antarctic Circumpolar Current is shifted northward in the Atlantic sector and southward in the Indian and Pacific sectors. Thereby differences in velocities of more than 1 cm/s are obtained, which is a relative alteration by 50–75%. Smaller increases of up to 0.4 cm/s are also obtained in the equatorial Pacific (50-150%) and at the east coast of Africa (500-700%).

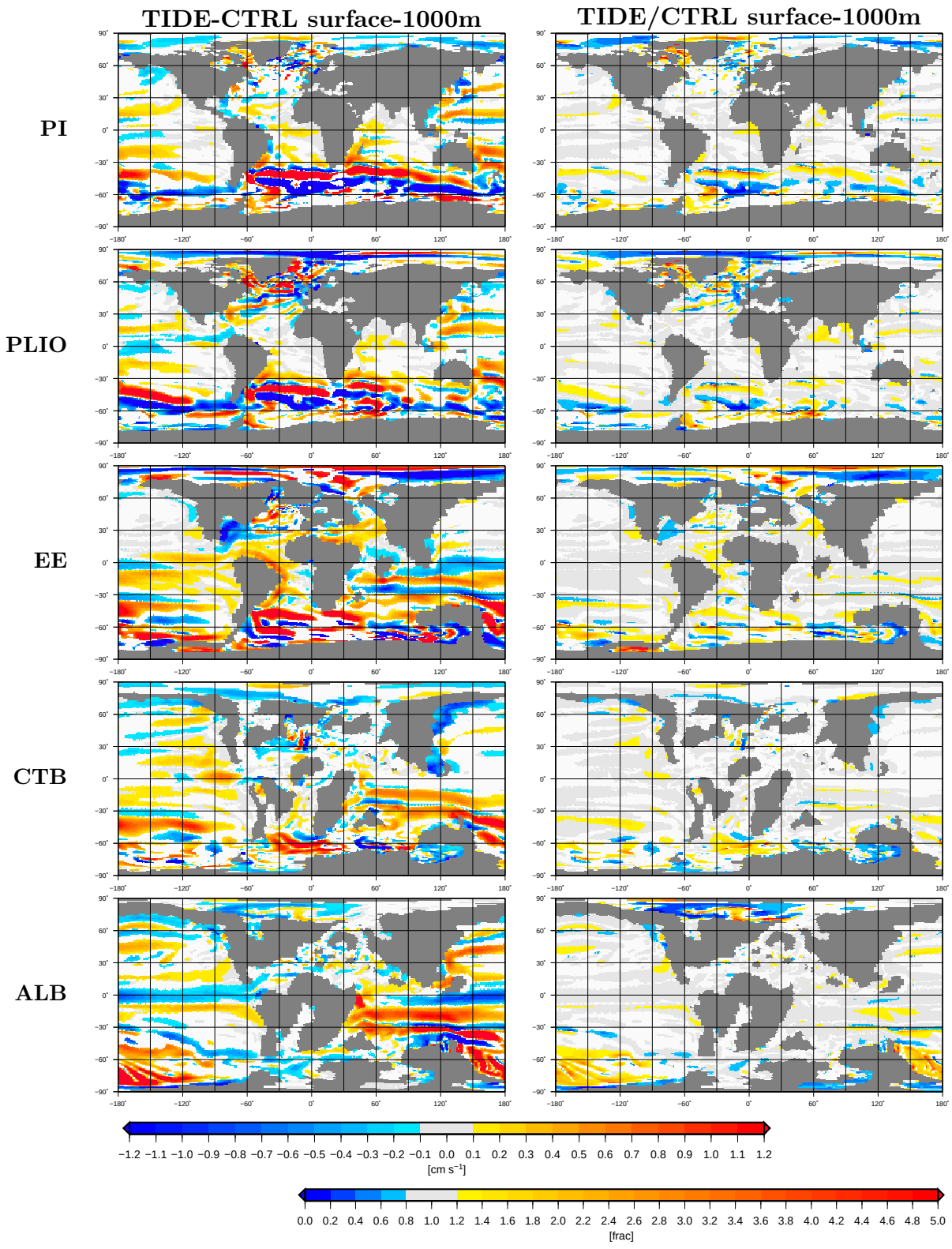

Figure 3: The absolute difference TIDE-CTRL (left) and fraction TIDE/CTRL (right) of horizontal velocities integrated over to upper 1000 m of the ocean for the pre-industrial period, the Early Pliocene, the Early Eocene, the CTB and the Early Albian. Statistically not significant differences are displayed in white.

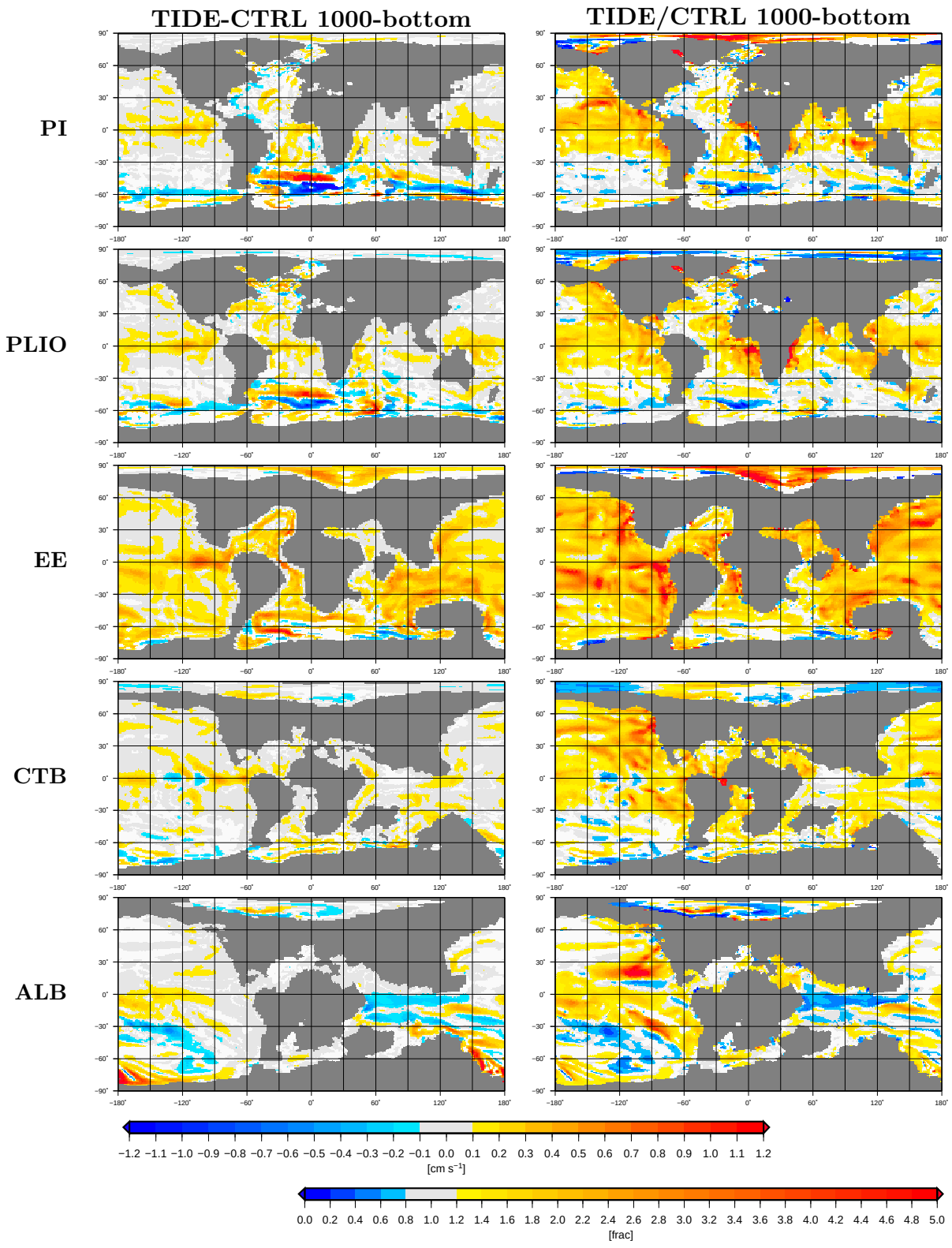

Figure 4: The absolute difference TIDE-CTRL (left) and fraction TIDE/CTRL (right) of horizontal velocities integrated from 1000 m depth to the ocean bottom for the pre-industrial period, the Early Pliocene, the Early Eocene, the CTB and the Early Albian. Statistically not significant differences are displayed in white.

Both absolute and relative changes in velocities in the pre-industrial period are similar to the Early Pliocene. The currents in the equatorial Pacific are further increased by 400–600%, while the currents at the African east coast are increased by only 200–250%.

As the tidal energy input suggests, the largest increase in relative velocities is simulated for the Early Eocene, where velocities are more than doubled in more than 35% of the lower ocean. The strongest relative reduction of velocities is obtained in the Early Albian, for which a reduction of more than 20% is simulated in over 15% of the lower ocean.

3.3 The influence of tides on temperatures

Tidally forced variations in heat advection, vertical mixing and atmospheric forcing modify the three-dimensional temperature distribution in the ocean (cf., Moon (2005); Lee et al. (2006); Holloway and Proshutinsky (2007)). Heat and momentum fluxes between ocean and atmosphere affect atmosphere dynamics. In consequence, sea ice, albedo, atmospheric pressure systems and winds are influenced by oceanic tides and nonlinearly modify atmospheric temperatures, as depicted in figure 5.

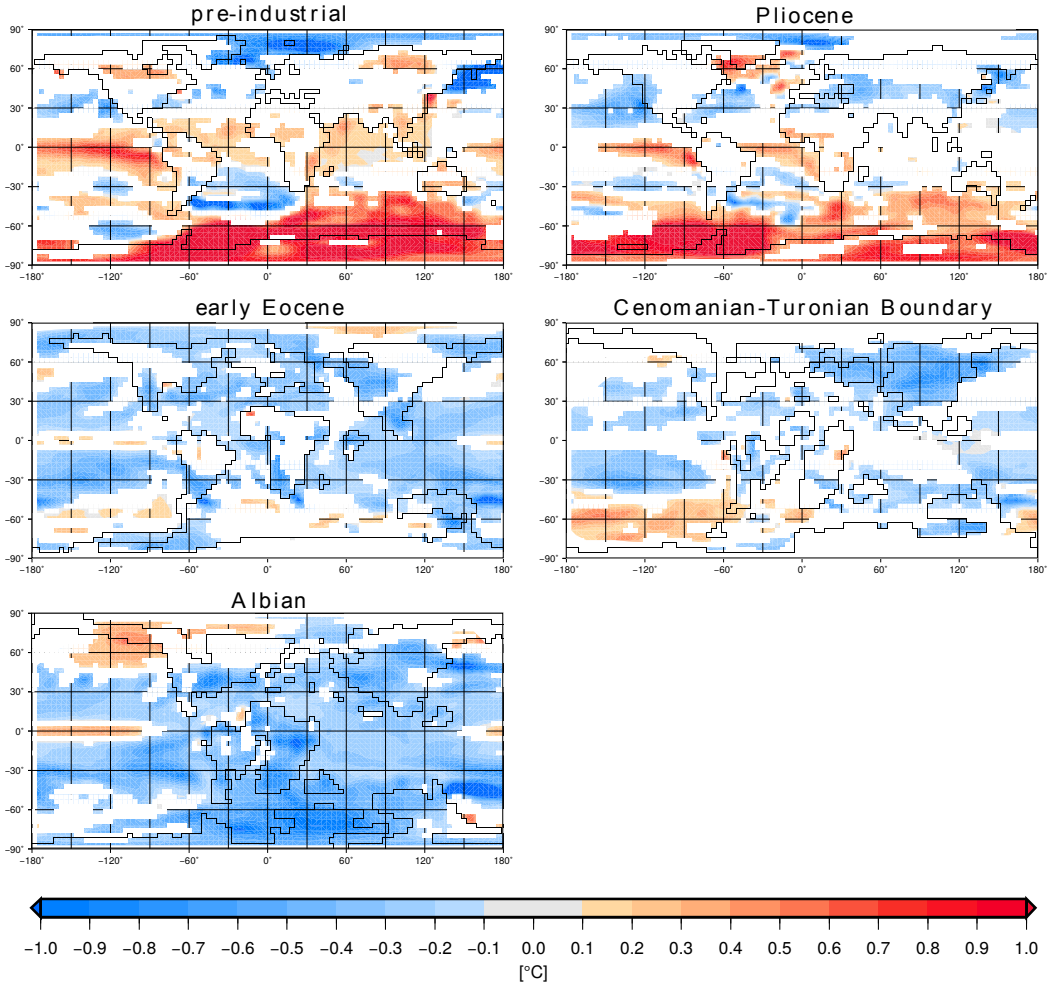

Figure 5: The difference TIDE-CTRL of atmospheric 2 m temperatures for the pre-industrial period, the Early Pliocene, the Early Eocene, the CTB and the Early Albian. Statistically not significant differences are displayed in white.

In the Early Albian, tidal dynamics significantly modify atmospheric 2 m temperatures locally between -2.2°C and 0.7°C with a global mean of -0.35°C. Changes are largest over the ocean, where sea surface temperatures are subject to direct modifications by altered surface currents and mixing. This is mainly the case in the Southern Ocean in the Pacific and Atlantic sectors where 2 m temperatures are changed by more than 1°C. Modifications of continental 2 m temperatures are largest in Africa, North America, Antarctica, and Alaska. The latter two temperature deviations are related to differences in albedo which stem from altered patterns in snow coverage. These differences in snowfall might be caused by a tidally induced warming of surrounding sea surface temperatures and a consequent increase in continental air temperatures. This may result in snow melt and a reduction of albedo, thus exercising a positive feedback on temperature increase. In Antarctica the opposite effects lead to decreased temperatures. This feedback is especially strong in Alaska and Antarctica, because these areas are covered in winter by a thin layer of snow and thus are sensitive to temperature alterations. Similar changes of albedo can also be observed at the entire north Pacific coast and northern Asia.

Both the CTB and the Early Eocene are subject to small changes of 2 m temperatures between -0.7°C an 0.5°C, with a global mean of -0.2°C. Modifications occur mostly over the ocean, where also sea surface temperatures are modified. However, large areas, especially over the continents, are not changed significantly.

The tidal shift of the ACC in the Early Pliocene is not only visible in the lower ocean, but also in the upper ocean. Thus more water is advected from the Southern Ocean to the Argentine Basin, contributing to a reduction of 2 m temperatures by more than 1°C. Feedback mechanisms between temperature and sea ice formation lead to a reduction of sea ice concentration by up to 30% and a warming of up to 2.5°C in the Weddell Sea and between 0.8°C and 1.5°C in the Pacific sector of the Southern Ocean. In the Arctic Ocean, on the other hand, sea ice concentration is increased by 8% and thereby 2 m temperatures reduced by 0.5–1.2°C.

The pre-industrial period is simulated as 3.5°C colder than the Early Pliocene. Sea ice concentration is hence higher and the feedback mechanisms between temperature and sea ice gain in importance. In the Weddell Sea a reduction of up to 30% of sea ice concentration is simulated which leads to an increase in 2 m temperature of 4°C. In the Atlantic and Indian Ocean sectors of the Southern Ocean, 2 m temperatures are increased by 1.4–2.4°C. Similar to the Early Pliocene, also in the pre-industrial period, sea ice concentration is reduced by tidal forcing in the Arctic Ocean, ensuing a reduction of 2 m temperatures by 1.7°C. In the North Pacific, sea surface temperatures are diminished by 1.6°C in the Bering Sea and by 2.4°C in the Sea of Okhotsk. These alterations in temperatures are transmitted to the atmosphere and reduce 2 m temperatures by 1.2–1.9°C. As in the Early Pliocene, the northward shift of the ACC into the South Atlantic contributes to a reduction of sea surface temperatures by more than 2°C.

4 Discussion

Reconstructing paleo-tides is limited by our restricted knowledge about (1) the position of Sun and Moon with respect to Earth, (2) deep ocean stratification, (3) position of shorelines, and (4) bathymetry (Egbert et al. (2004)). However, only some of these limitations can be quantified. (1) The orbital parameters of Earth and Moon (e.g., eccentricity, length of semi-major axis, angular velocity) vary periodically and non-periodically over time (Laskar et al. (2004)). The estimates of the positions of Sun and Moon with respect to Earth several million years ago are therefore subject to uncertainty (Laskar et al. (2011)). Weber (2016) simulated the M_2 amplitude over several time-slices with present-day and reconstructed paleo orbital parameters.

The global mean of the magnitude difference between the two orbital settings increased quasi-linearly in time. Largest difference was obtained with 6% for the Albian, with the main effect being the distance between Moon and Earth. Using present-day orbital parameters leads for all time-slices to lower M_2 amplitudes than using paleo orbital parameters. The quantitative results of this study might therefore be considered a lower bound of the effects of tides on the climate system and the qualitative conclusions are not affected by the choice between present-day and paleo orbital parameters. (2) In this study we use a spun-up coupled atmosphere-ocean model wherefore we may assume that the deep ocean stratification is as representative of the prevailing climatic conditions of each time-slice as possible with current climate models. (3) The position of shorelines at a given time are quite uncertain and controversially discussed for some of the time-slices, e.g., the timing of the opening of the Drake Passage in the Paleocene/ Eocene (Lawver and Gahagan (2003); Livermore et al. (2005); Ghiglione et al. (2008)). (4) Also the bathymetries are often only crudely known, which becomes most problematic for time-slices with large areas of shallow water, e.g. the epicontinental seas during the Cretaceous. The uncertainties in the latter two boundary conditions result in unquantifiable uncertainties in tidal dynamics that we can only assess by comparison to other model studies and in-situ data (e.g., Green and Huber (2013); Ray (2013)). For this reason, the conclusions drawn in this study can only be qualitative. All quantitative results should hence be regarded as a way of comparing variables from different time-slices on the way to deducting qualitative conclusions.

Processes of tidal mixing are commonly not included in OGCMs (Müller (2013)). In shelf areas strong tidal currents increase vertical velocities and induce thereby vertical mixing. This process can be included into an OGCM either by explicitly forcing tides (e.g., Müller et al. (2010))

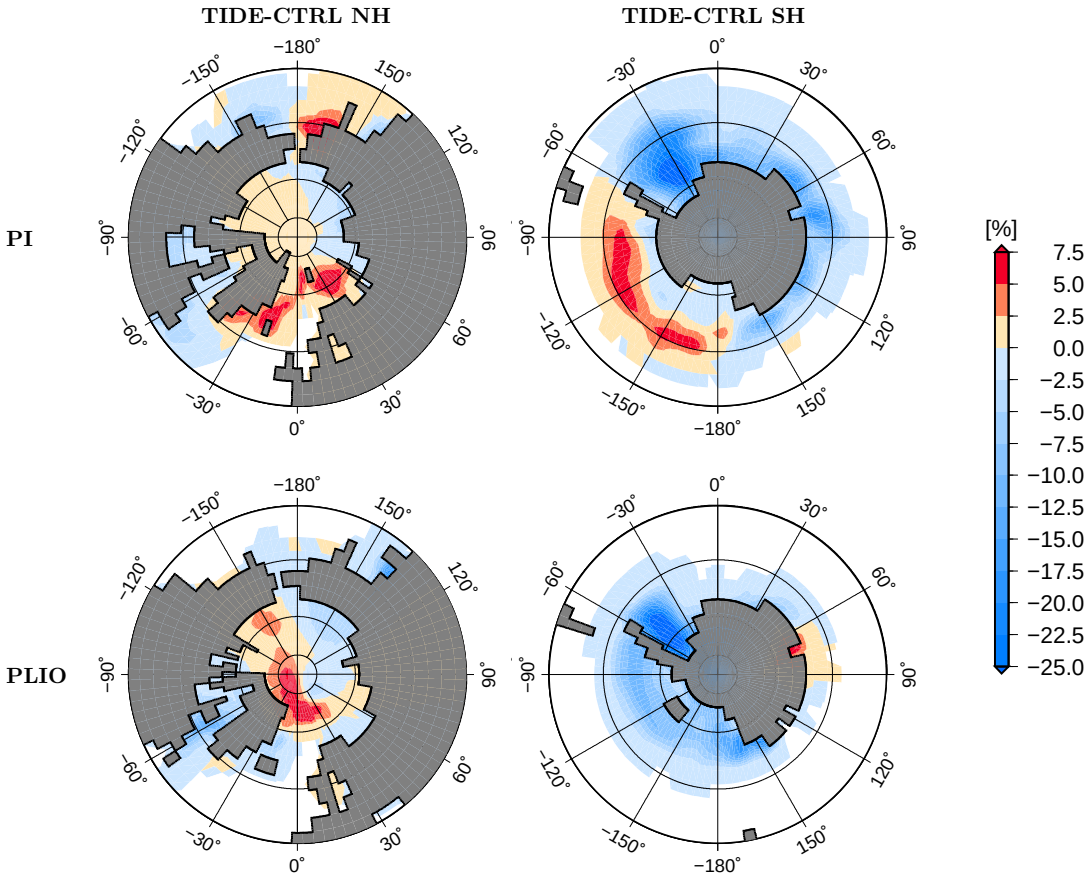

Figure 6: The difference TIDE-CTRL of sea ice concentration for the northern and southern hemispheres of the pre-industrial period and the Early Pliocene.

or by including tidal currents from a different model (e.g., Lee et al. (2006)). Tidal mixing in the deep ocean is caused by generation and breaking of internal waves over rough topography (Garrett (2003)). This process is parametrized in ocean models depending on tidal velocities, topographic roughness and vertical stratification (St. Laurent et al. (2002)).
In this study tides are forced explicitly in the ocean model. Tidal currents hence increase the vertical shear of horizontal velocities through bottom friction which acts on the vertical mixing scheme and thereby generates tidal mixing. This effect is mainly of importance in shelf areas. However, no parametrization of the generation of tidal waves is considered. Bathymetry and shorelines are known only very crudely for paleo-times and no estimate of topographic roughness is available. The existing parametrization schemes for internal tides can therefore not be applied consistently in paleo-simulations. Considering internal tides is expected to intensify vertical mixing and thus probably increase the differences between TIDE and CTRL further. The here presented results might therefore be regarded as a lower estimate of tidal impact on velocities, 2 m temperatures and sea ice concentration.

Former studies about tides in paleo-oceans focused mainly on tidal dissipation. Here we complement these studies by including the interaction between the ocean general circulation, tidal dynamics and feedbacks with the atmosphere. Tidal systems between the Cretaceous and the Early Pliocene have only been modeled by Green and Huber (2013), who simulated tides during the Early Eocene with the Oregon State University Tidal Inversion System (OTIS). The model solves linearized shallow water equations with an additional term for tidal energy conversion of the M_2 tide. The energy conversion scheme depends on the prescribed stratification of the ocean. While the location of amphidromic points is independent of the stratification, tidal amplitudes are influenced by stratification. Amplitudes of the M_2 tide are simulated larger with pre-industrial stratification than with Early Eocene stratification. Largest amplitudes are obtained in both simulations in the central and north Pacific, the northern Central American Seaway and close to Australia. Apart from stratification, the simulations by Green and Huber (2013) also differ from EETIDE in bathymetry and continental distribution. This is due to large uncertainties in the reconstruction of bathymetry and the ongoing discussion about the exact timing of the opening of the Drake Passage (e.g., Lawver and Gahagan (2003); Livermore et al. (2005); Ghiglione et al. (2008)). While an exchange of surface water between the South Atlantic and the Pacific Ocean might have been possible in the Early Eocene, a flow of intermediate and deep water was not possible. In order to prevent the onset of a proto-ACC, the Drake Passage is closed in EETIDE (following Livermore et al. (2005); Scher and Martin (2006); DeConto (2009)) while they are open in Green and Huber (2013). Since proxy data suggest an exchange of water between the Arctic Ocean and its surrounding ocean basins in the Early Eocene (Iakovleva and Heilmann-Clausen (2007); Gleason et al. (2009)), the Fram and Bering Straits are open in EETIDE while they are closed in Green and Huber (2013). Furthermore, in Green and Huber (2013) New Zealand has been formed until the Early Eocene, while it does not exist in the reconstruction used for EETIDE (cf., Sewall et al. (2000)). The latter difference leads to a shift from highest amplitudes surrounding Australia in EETIDE to high amplitudes surrounding New Zealand in Green and Huber (2013). Moreover, the open Drake and Tasman Passages permit tidal waves to travel freely along the Australian coast in Green and Huber (2013). In EETIDE, these closed gateways inhibit the propagation of tidal waves, thus inducing the formation of a Kelvin wave at the Australian coast.

Sea ice and glaciers can alter the geometry of ocean basins on much shorter time-scales than plate tectonics. They had a large influence during the last glacial maximum (LGM), where extended ice sheets and thereby reduced sea level changed the position of amphidromic points and increased the amplitudes of the M_2 tide by up to 70 cm (Thomas and Sündermann (1999); Egbert et al. (2004); Griffiths and Peltier (2009)). Also in present-day oceans, sea ice is of

importance when simulating tides in the polar oceans. In PITIDE a reduction of up to 30% of sea ice concentration is simulated in the Weddell sea. Tidally increased diffusion mixes water masses stronger in PITIDE than in PICTRL. Since in the Southern Ocean surface waters are colder than deep waters, this leads to a warming of the upper 200 m of the Weddell Sea in PITIDE and a cooling of the lower 200 m. Thereby less sea ice is formed in PITIDE than in PICTRL and the sea ice concentration is diminished. Furthermore, thermal insulation of the sea ice cover is reduced, hence increasing the latent heat flux from the ocean to the atmosphere during austral winter. Thereby 2 m temperatures are increased, which inhibits the formation of sea ice during winter and further reduces sea ice concentration. This feedback mechanism leads in the Weddell Sea to an annual mean reduction of sea ice concentration of 30% and an increase in 2 m temperature of 4°C. Koentopp et al. (2005) modeled tides and sea ice in the Weddell Sea with the regional, barotropic tidal model Circum-Antarctic Tidal Simulation (CATS00.2) with a resolution of $1/4° \times 1/12°$. Similar to PITIDE, they find a decrease in sea ice concentration by up to 20% when including tidal forcing into their model. They attribute this reduction to advection by the mean ice drift and a warming of the upper ocean due to increased mixing with deeper water and an increased heat flux from atmosphere to ocean during summer.
In the Arctic Ocean, PITIDE models a decrease in temperature of up to 1.4°C in 75 m depth (not shown) between Svalbard and Greenland, and very limited changes in the remaining ocean basin. This compares well with a study by Holloway and Proshutinsky (2007), who used the Arctic Ice/Ocean Model AIM with a resolution of 55 km to investigate the influence of ocean tides on sea ice and ocean temperature. They found a cooling of approximately 2°C in 80 m depth in the Arctic Ocean along the axis Greenland-Svalbard-Nowaja Semlja when including tidal forcing into their ocean model. The western Arctic Ocean did not exhibit strong temperature anomalies in their model setup.

In PITIDE the North Atlantic is simulated as 1.5°C colder when including tides than without their consideration. A similar result is obtained by Müller et al. (2010) with the model ECHAM5/MPIOM with a higher resolution than in our setup. In their simulation, the North Atlantic Current is simulated weaker and more accurate when including tides into the model. Hence, less heat is transported from the tropical Atlantic into the North Atlantic and therefore by up to 2°C colder waters are modeled. In contrast to these two results, Lee et al. (2006) obtained with the coupled atmosphere–ocean model GFDL CM2.0 with a parametrization of barotropic tidal mixing a by up to 2°C warmer sea surface in the Labrador Sea. The authors attribute this warming to a shift of the central axis of the Gulf Stream.

5 Conclusions

We presented the results of a simultaneous simulation of ocean general circulation and tidal dynamics with a coupled atmosphere-ocean model for five time-slices ranging from the Early Albian to present day. We have highlighted a general chain of processes and feedback mechanisms on how tidal dynamics can influence climate. We furthermore have described the effects as they are simulated in the coupled atmosphere-ocean model ECHAM5/MPIOM. A detailed analysis of the physical process behind individual phenomena of each time-slice is subject of further research.
The tidal systems change over time due to the evolution of ocean basin geometry in response to plate tectonics. Largest amplitudes of the M_2 tide, and thus largest tidal potential energy (TPE), are simulated for the Early Eocene, where the TPE is almost twice as high as in any other time-slice. The response of the ocean to tidal forcing has specific characteristics in each time-slice. The Early Albian is the only time-slice in which horizontal ocean velocities are considerably reduced due to tidal dynamics. This is mainly the case in the Indo-Pacific

Throughflow, where velocities are reduced by up to 50% in the lower Indian Ocean. In the Early Eocene, on the other hand, tidal dynamics modify velocities by more than 100% in more than 35% of the lower ocean, and by more than 200% in 10% of the ocean. Enhanced horizontal velocities also increase the meridional overturning circulation in the Early Eocene. In the CTB the TPE is with a value of 719 PJ smaller than in the other time-slices and thus the response of the ocean to tidal forcing is majorly confined to velocity alterations by less than 50% and modifications of atmospheric 2 m temperatures by -0.7°C to 0.5°C. In contrast, in the pre-industrial period and in the Pliocene 2 m temperatures are increased by tidal dynamics by more than 4°C in the Weddell Sea.

Present-day and Pliocene bathymetries mainly differ with respect to the closing of the Central American Seaway. However, this small change significantly affects resonance conditions in the Atlantic and the Pacific Oceans and is responsible for the formation of larger amplitudes at the Brazilian coast in the Pliocene. The effect of slight modifications in bathymetry is also visible when comparing Green and Huber (2013) and EETIDE. The results presented here are subject to uncertainties originating from uncertainties in reconstructed bathymetries and shorelines. The quantitative results should therefore be considered as a means to derive qualitative and comparative conclusions. According to our results the ocean's response to tidal forcing differs strongly between time-slices. A time-independent parametrization of tidal effects is therefore not advised. However, tidally induced modifications of the ocean's general circulation are too large to be neglected and have to be considered in paleo-climate simulations as a source of uncertainty for model and proxy comparison. In contrast to paleo-bathymetries, the present-day bathymetry is well known and tidal dynamics could therefore be included properly into present-day climate simulations and into climate projections.

6 Acknowledgements

The model experiments were carried out on the supercomputing system of the German Climate Computation Centre (DKRZ) Hamburg. This study is funded by the Deutsche Forschungsgemeinschaft (DFG) under grants TH 864/11-1 and TH 864/11-2 as part of the priority program SPP 1375 SAMPLE (South Atlantic Margin Processes and Links with onshore Evolution). We thank three anonymous reviewers for their helpful comments.

References

Accad, Y. and Pekeris, C. L. (1978). Solution of the Tidal Equations for the M_2 and S_2 Tides in the World Oceans from a Knowledge of the Tidal Potential Alone. *Philosophical Transactions of the Royal Society A: Mathematical, Physical and Engineering Sciences*, 290(1368):235–266.

Archer, A. W. (1996). Panthalassa: paleotidal resonance and a global paleocean seiche. *Paleoceanography*, 11(5):625–632.

Aucour, A.-M., Gomez, B., Sheppard, S. M., and Thévenard, F. (2008). $\delta^{13}C$ and stomatal number variability in the Cretaceous conifer Frenelopsis. *Palaeogeography, Palaeoclimatology, Palaeoecology*, 257(4):462–473.

Brierley, C. M. and Fedorov, A. V. (2011). Tidal mixing around Indonesia and the Maritime continent: Implications for paleoclimate simulations. *Geophysical Research Letters*, 38(24).

Cunningham, S., Alderson, S. G., King, B. A., and Brandon, M. A. (2003). Transport and variability of the Antarctic Circumpolar Current in Drake Passage. *Journal of Geophysical Research*, 108(C5):8084.

DeConto, R. M. (2009). Plate tectonics and climate change. In Gornitz, V., editor, *Encyclopedia of Paleoclimatology and Ancient Environments: Encyclopedia of Earth Sciences Series*, pages 1049–1064. Springer.

Duffett-Smith, P. (1986). *Astronomy with your personal computer*. Cambridge Univ. Press, Cambridge.

Egbert, G. D., Ray, R. D., and Bills, B. G. (2004). Numerical modeling of the global semidiurnal tide in the present day and in the last glacial maximum. *Journal of Geophysical Research*, 109:1–15.

Fletcher, B. J., Brentnall, S. J., Anderson, C. W., Berner, R. A., and Beerling, D. J. (2008). Atmospheric carbon dioxide linked with Mesozoic and early Cenozoic climate change. *Nature Geoscience*, 1(1):43–48.

Garrett, C. (2003). Internal tides and ocean mixing. *Science (New York, N.Y.)*, 301:1858–9.

Ghiglione, M. C., Yagupsky, D., Ghidella, M., and Ramos, V. A. (2008). Continental stretching preceding the opening of the Drake Passage: Evidence from Tierra del Fuego. *Geology*, 36(8):643.

Gleason, J. D., Thomas, D. J., Moore Jr, T. C., Blum, J. D., Owen, R. M., and Haley, B. A. (2009). Early to middle Eocene history of the Arctic Ocean from Nd-Sr isotopes in fossil fish debris, Lomonosov Ridge. *Paleoceanography*, 24(2).

Gotlib, V. Y. and Kagan, B. A. (1985). A Reconstruction of the Tides in the Paleocean: Results of a Numerical Simulation. *Deutsche hydrographische Zeitung*, H2:43–67.

Green, J. A. M. and Huber, M. (2013). Tidal dissipation in the early Eocene and implications for ocean mixing. *Geophysical Research Letters*, 40(11):2707–2713.

Griffiths, S. D. and Peltier, W. R. (2009). Modeling of Polar Ocean Tides at the Last Glacial Maximum: Amplification, Sensitivity, and Climatological Implications. *Journal of Climate*, 22(11):2905–2924.

Haworth, M., Hesselbo, S. P., McElwain, J. C., Robinson, S. A., and Brunt, J. W. (2005). Mid-Cretaceous pCO_2 based on stomata of the extinct conifer Pseudofrenelopsis (Cheirolepidiaceae). *Geology*, 33(9):749.

Haywood, A. M., Dowsett, H. J., Robinson, M. M., Stoll, D. K., Dolan, a. M., Lunt, D. J., Otto-Bliesner, B., and Chandler, M. (2010). Pliocene Model Intercomparison Project (PlioMIP): experimental design and boundary conditions (Experiment 2). *Geoscientific Model Development*, 4(3):227–242.

Holloway, G. and Proshutinsky, A. (2007). Role of tides in Arctic ocean/ice climate. *Journal of Geophysical Research*, 112:C04S06.

Hong, S. K. and Lee, Y. I. (2012). Evaluation of atmospheric carbon dioxide concentrations during the Cretaceous. *Earth and Planetary Science Letters*, 327-328:23–28.

Huber, M. and Sloan, L. C. (2001). Heat transport, deep waters, and thermal gradients: Coupled simulation of an Eocene greenhouse climate. *Geophysical Research Letters*, 28(18):3481–3484.

Iakovleva, A. I. and Heilmann-Clausen, C. (2007). Wilsonidium Pechoricum new species - a new Dinoflagellate species with unusual asymmetry from the Paleocene/Eocene Transition. *Journal of Paleontology*, 81(5):1020–1030.

Jungclaus, J. H. (2007). MPI-M Earth System Modelling Framework: millennium control experiment. World Data Center for Climate. CERA-DB "mil0001".

Koentopp, M., Eisen, O., Kottmeier, C., Padman, L., and Lemke, P. (2005). Influence of tides on sea ice in the Weddell Sea: Investigations with a high-resolution dynamic-thermodynamic sea ice model. *Journal of Geophysical Research*, 110:C02014.

Laskar, J., Fienga, A., Gastineau, M., and Manche, H. (2011). La2010: A new orbital solution for the long term motion of the Earth. *Astronomy And Astrophysics*, 532(A89).

Laskar, J., Robutel, P., Joutel, F., Gastineau, M., Correia, A. C. M., and Levrard, B. (2004). A long term numerical solution for the insolation quantities of the Earth. *Astronomy and Astrophysics*, 428(1):261–285.

Lawver, L. A. and Gahagan, L. M. (2003). Evolution of Cenozoic seaways in the circum-Antarctic region. *Palaeogeography, Palaeoclimatology, Palaeoecology*, 198:11–37.

Lee, H.-C., Rosati, A., and Spelman, M. J. (2006). Barotropic tidal mixing effects in a coupled climate model: Oceanic conditions in the Northern Atlantic. *Ocean Modelling*, 11:464–477.

Livermore, R., Nankivell, A., Eagles, G., and Morris, P. (2005). Paleogene opening of Drake Passage. *Earth and Planetary Science Letters*, 236(1-2):459–470.

Lunt, D. J., Jones, T. D., Heinemann, M., Huber, M., LeGrande, A., Winguth, A., Loptson, C., Marotzke, J., Roberts, C. D., Tindall, J., Valdes, P. J., and Winguth, C. (2012). A model–data comparison for a multi-model ensemble of early Eocene atmosphere–ocean simulations: EoMIP. *Climate of the Past*, 8(5):1717–1736.

Marsland, S., Haak, H., Jungclaus, J. H., Latif, M., and Röske, F. (2003). The Max-Planck-Institute global ocean/sea ice model with orthogonal curvilinear coordinates. *Ocean Modelling*, 5(2):91–127.

McCarthy, G., Smeed, D., Johns, W., Frajka-Williams, E., Moat, B., Rayner, D., Baringer, M., Meinen, C., Collins, J., and Bryden, H. (2015). Measuring the Atlantic Meridional Overturning Circulation at 26°N. *Progress in Oceanography*, 130:91–111.

Montenegro, Á., Eby, M., Weaver, A. J., and Jayne, S. R. (2007). Response of a climate model to tidal mixing parameterization under present day and last glacial maximum conditions. *Ocean Modelling*, 19(3-4):125–137.

Moon, I.-J. (2005). Impact of a coupled ocean wave-tide-circulation system on coastal modeling. *Ocean Modelling*, 8(3):203–236.

Müller, M. (2013). On the space- and time-dependence of barotropic-to-baroclinic tidal energy conversion. *Ocean Modelling*, 72:242–252.

Müller, M., Haak, H., Jungclaus, J. H., Sündermann, J., and Thomas, M. (2010). The effect of ocean tides on a climate model simulation. *Ocean Modelling*, 35(4):304–313.

Parke, M. E. (1982). O_1, P_1, N_2 models of the global ocean tide on an elastic earth plus surface potential and spherical harmonic decompositions for M_2, S_2, and K_1. *Marine Geodesy*, 6(1):35–81.

Passalia, M. G. (2009). Cretaceous pCO_2 estimation from stomatal frequency analysis of gymnosperm leaves of Patagonia, Argentina. *Palaeogeography, Palaeoclimatology, Palaeoecology*, 273(1-2):17–24.

Pearson, P. N. and Palmer, M. R. (2000). Atmospheric carbon dioxide concentrations over the past 60 million years. *Nature*, 406(6797):695–9.

Ray, R. D. (2013). Precise comparisons of bottom-pressure and altimetric ocean tides. *Journal of Geophysical Research: Oceans*, 118(9):4570–4584.

Roeckner, E., Bäuml, G., Bonaventura, L., Brokopf, R., Esch, M., Giorgetta, M., Hagemann, S., Kirchner, I., Kornblueh, L., Rhodin, A., Schlese, U., Schulzweida, U., and Tompkins, A. (2003). The atmospheric general circulation model ECHAM5: Part 1: Model description. Technical Report No. 349, DKRZ.

Roeckner, E., Brokopf, R., Esch, M., Giorgetta, M., Hagemann, S., Kornblueh, L., Manzini, E., Schlese, U., and Schulzweida, U. (2004). The Atmospheric General Circulation Model ECHAM5: Part II. Technical Report No. 354, DKRZ.

Royer, D. L. (2006). CO_2-forced climate thresholds during the Phanerozoic. *Geochimica et Cosmochimica Acta*, 70(23):5665–5675.

Royer, D. L. (2014). Atmospheric CO_2 and O_2 During the Phanerozoic: Tools, Patterns, and Impacts. In *Treatise on Geochemistry*, chapter 6.11, pages 251–267. Elsevier Ltd., 2 edition.

Royer, D. L., Wing, S. L., Beerling, D. J., Jolley, D. W., Koch, P. L., Hickey, L. J., and Berner, R. A. (2001). Paleobotanical evidence for near present-day levels of atmospheric CO$_2$ during part of the tertiary. *Science (New York, N.Y.)*, 292(5525):2310–3.

Scher, H. D. and Martin, E. E. (2006). Timing and climatic consequences of the opening of Drake Passage. *Science (New York, N.Y.)*, 312(5772):428–30.

Schiller, A. (2004). Effects of explicit tidal forcing in an OGCM on the water-mass structure and circulation in the Indonesian throughflow region. *Ocean Modelling*, 6:31–49.

Schmittner, A., Green, J. a. M., and Wilmes, S.-B. (2015). Glacial ocean overturning intensified by tidal mixing in a global circulation model. *Geophysical Research Letters*, pages 4014–4022.

Sewall, J. O., Sloan, L. C., Huber, M., and Wing, S. L. (2000). Climate sensitivity to changes in land surface characteristics. *Global and Planetary Change*, 26(4):445–465.

Sewall, J. O., van de Wal, R. S. W., van der Zwan, K., van Oosterhout, C., Dijkstra, H. A., and Scotese, C. R. (2007). Climate model boundary conditions for four Cretaceous time slices. *Climate of the Past*, (3):647–657.

St. Laurent, L. C., Simmons, H. L., and Jayne, S. R. (2002). Estimating tidally driven mixing in the deep ocean. *Geophysical Research Letters*, 29(23):2106.

Thomas, D. J., Korty, R., Huber, M., Schubert, J. A., and Haines, B. (2014). Nd isotopic structure of the Pacific Ocean 70 - 30 Ma and numerical evidence for vigorous ocean circulation and ocean heat transport in a greenhouse world. *Paleoceanography*, pages 454–469.

Thomas, M. and Sündermann, J. (1999). Tides and tidal torques of the world ocean since the last glacial maximum. *Journal of Geophysical Research*, 104(C2):3159–3183.

Thomas, M., Sündermann, J., and Maier-Reimer, E. (2001). Consideration of ocean tides in an OGCM and impacts on subseasonal to decadal polar motion excitation. *Geophysical Research Letters*, 28(12):2457–2460.

Uenzelmann-Neben, G., Weber, T., Gruetzner, J., and Thomas, M. (2016). Tectonophysics Transition from the Cretaceous ocean to Cenozoic circulation in the western South Atlantic — A twofold reconstruction. *Tectonophysics*.

Weber, T. (2016). *Impact of ocean tides on the climate system during the pre-industrial period, the early Eocene, and the Albian.* PhD thesis, Department of Earth Sciences, Freie Universität Berlin,http://www.diss.fu-berlin.de/diss/servlets/MCRFileNodeServlet/FUDISS_derivate_000000018340/Dissertation_TWeber.pdf

Weber, T. and Thomas, M. (2017). Influence of ocean tides on the general ocean circulation in the early Eocene. *Paleoceanography*, 32(6):553–570.

White, T. S., Witzke, B. J., and Ludvigson, G. A. (2000). Evidence for an Albian Hudson arm connection between the Cretaceous Western Interior Seaway of North America and the Labrador Sea. *Geological Survey of America Bulletin*, 112(9):1342–1355.

Wunsch, C. (2002). What is the thermohaline circulation? *Science*, 298(5596):1179–81.

Wunsch, C. (2005). Speculations on a schematic theory of the Younger Dryas. *Journal of Marine Research*, (63):315–333.

Wunsch, C. (2016). Tides of Global Ice-Covered Oceans. *Icarus*, 274:122–130.

Zeebe, R. E., Zachos, J. C., and Dickens, G. R. (2009). Carbon dioxide forcing alone insufficient to explain Palaeocene–Eocene Thermal Maximum warming. *Nature Geoscience*, 2(8):576–580.